IEEE Access
Multidisciplinary | Rapid Review | Open Access Journal

Received August 26, 2020, accepted September 11, 2020, date of publication September 21, 2020, date of current version October 1, 2020.

Digital Object Identifier 10.1109/ACCESS.2020.3025152

An Effective Control Scheme for Multimodal SSR Suppression via VSC-Based Controller

XIAOTIAN YUAN, (Student Member, IEEE), ZHENGCHUN DU, (Senior Member, IEEE), XIAOFANG WU, GUIHONG WU, SHUAI GAO, FENG ZENG, AND CHONGTAO LI

School of Electrical Engineering, Xi'an Jiaotong University, Xi'an 710049, China

Corresponding author: Xiaotian Yuan (yxt2013@stu.xjtu.edu.cn)

This work was supported in part by the National Key Research and Development Program of China under Grant 2017YFB0902000, and in part by the Science and Technology Project of State Grid under Grant SGXJ0000KXJS1700841.

ABSTRACT Multimodal sub-synchronous resonance (SSR) induced by the interactions between the generator shafts and the fixed series capacitors has become a serious threat for the power system. To overcome this, a voltage source converter (VSC) based controller for multimodal SSR suppression, named sub-synchronous resonance dynamic suppressor (SSRDS), is presented and analyzed in this paper. The controller is placed at the point of common coupling (PCC) of the power plant for multi-generator SSR suppression purpose so that the investment costs can be minimized while making sure the requirements of the SSR damping. To quantify the contribution of SSRDS to the SSR damping, the damping torque analysis is carried out, which can reveal the influences of the operating conditions and the correlated control parameters on the damping performance. Furthermore, to avoid the negative affects between the different TMs in close range as well as maximize the damping ability of SSRDS, the parameters tuning method of the mode filters and the gain and phase shifters are proposed. A detailed nonlinear simulation model is established in PSCAD/EMTDC based on the Jinjie series compensated transmission system located in China. The damping torque analysis, the eigenvalues analysis and the simulation results have fully demonstrated the effectiveness and the robustness of the proposed SSRDS for multi-generator and multimodal SSR suppression under both small and large disturbances in various operating conditions.

INDEX TERMS Sub-synchronous resonance (SSR), sub-synchronous resonance dynamic suppressor (SSRDS), torsional mode, VSC, multimodal SSR.

I. INTRODUCTION

As a simple and economic solution, the series compensation transmission system has been widely utilized in practical power system [1] in order to enhance system stability and promote the transmission capacity limitation. Notably, this scheme may bring potential sub-synchronous resonance (SSR) problems to the system, which might cause shaft fatigue for the generators and eventually lead to the serious unstable issues for the overall stability of the power grid [2].

SSR is a phenomenon that occurs when the electrical resonance frequency of the power grid and the natural frequency of the generator shaft are complementary, whose oscillation frequency is normally below the synchronous frequency. The mechanism of SSR has been deeply investigated in [3]. Recently, the popularity of this topic has once again increased in industry as SSR problems becomes more prominent due to the continuous expansion of the modern power system. For example, the SSR risks of Jinjie series compensated transmission system [4] in China is considerable given the recent installations of new large-capacity generators and new transmission lines.

The associate editor coordinating the review of this manuscript and approving it for publication was Yonghao Gui.

A. RELATED WORKS

In order to mitigate and suppress SSR, several control schemes have been proposed in [4]–[7] and [9]–[28]. Generally speaking, the above control schemes can be categorized into two classes. The first class in [5]–[7] and [9]–[12] can be called as the grid-side suppression schemes. The thyristor-controlled series capacitor (TCSC) based damping scheme was proposed in [5], [6], which suppresses SSR by adjusting the series compensation in sub-synchronous

This work is licensed under a Creative Commons Attribution 4.0 License. For more information, see https://creativecommons.org/licenses/by/4.0/

frequency range. However, the dynamic performance of TCSC is highly related to the operation conditions and the signals which reflect torsional modes cannot be easily obtained since the TCSC is normally installed away from the generators. A sub-synchronous oscillation damping controller (SODC) was reported in [7], which can be utilized in the conventional line-commutated-converter high voltage direct current (LCC-HVDC) transmission system for SSR damping. With the development of VSC technology [8], the SSR damping schemes can also be employed in the VSCs-embedded systems. References [9]–[11] proposed SSR damping controls for VSC-HVDC via regulating active and reactive output power of the VSC stations. Several effective nonlinear controllers [12]–[15] have been employed in the VSC based wind turbines (WT) for the purpose of Sub-Synchronous Control Interactions (SSCI) mitigation.

Given that the most severe victims of SSR are the generators, another class of the damping controls called as generator-side suppression schemes were proposed in [16]–[28], whose control effects are more direct for the generator shafts. The negative filters placed at the generator terminal for SSR damping were presented in [16]–[18]. They are effective but the parameter tune of these schemes are time-consuming and the investment costs are relatively high. The multimodal SSR was successfully mitigated with the help of supplementary excitation damping controller (SEDC) in [19], [20]. Regrettably, the damping performance of SEDC is limited by the capacity of the excitation system. A variable frequency drives based SSR damping control was proposed in [21] by making use of the motor loads of the power plants. The static synchronous compensators (STATCOM) based control schemes were also recommended in [22], [23]. These control schemes can be utilized for the SSR damping purpose. However, the primary functions of above schemes [22], [23] are the same as the traditional STATCOM, i.e., giving the fundamental reactive power support and voltage support for the power grid rather than SSR damping. The above control schemes in [19]–[23] can be regarded as the tiny modification on the existing power equipment of the power system, whose SSR damping ability is an auxiliary function and is restricted by other requirements of the power equipment.

To achieve the direct and independent control effects, plenty of dedicated SSR damping controllers placed at generator side are reported in [4], [24]–[28]. The static var compensator based sub-synchronous damping control (SVC-SSDC) was designed and put into practice in [4], [24], which contributes to the three-mode SSR mitigation in the early Jinjie Power Plant. A family of sub-synchronous dampers (SSDs), which provides SSR damping support via controlled injection of super-synchronous and sub-synchronous currents, was proposed in [25]. This work was followed by the generator terminal sub-synchronous damper (GTSSD), which utilized the VSC for damping multimodal SSR [26]. The performance of the GTSSD was also verified by experiments in Shangdu Power Plant in China. The current tracking controls of the controllers in [25], [26] were all performed in the three-phase stationary coordinate system. References [27], [28] proposed a VSC based controller for mitigating intermittent sub-synchronous oscillation (ISSO) caused by the interactions between the generator shafts and LCC-HVDC. The SSR mitigation mechanism of the controllers in [25]–[28] are similar to a certain extent. They provide SSR damping support by modulating reactive damping current based on the signals which reflect the torsional modes (TMs). However, they are all installed at the bus with low voltage and are only effective for the targeted single generator. These control schemes may be expensive for the power plants with multi-generator since each generator should be equipped with a dedicated controller and several backup controllers for the security purpose in practical applications.

As documented in [4], [24], the SSR problems of early Jinjie Power Plant have been well solved with the help of SVC-SSDC. However, with the new installations of large-capacity generators and transmission lines, the original designed SVC-SSDC may not be suitable for satisfying the new requirements of SSR suppression of Jinjie Power Plant. Besides, since the effective capacity of SVC-SSDC for SSR mitigation is limited by the plenty of harmonic current generated by the thyristors [4], it may not be an economical SSR suppression approach. Consequently, it's essential for making up novel control scheme to mitigate the multimodal SSR in Jinjie Power Plant. The comparisons between the SVC-SSDC and SSRDS will be presented in the case study.

B. MAIN CONTRIBUTION

This paper introduces an improved VSC based controller for multimodal and multi-generator SSR suppression, which is named as SSRDS. It has following advantages: 1) the SSRDS is an independent device and is dedicatedly designed for SSR suppression rather than voltage support, which will only be activated when SSR occurs; 2) the parameters tuning method of the mode filters and the gain and phase shifters can guarantee that the negative impacts from the interactions between the different TMs in close range can be minimized and the damping capability of SSRDS can be maximized; 3) the controller is placed at the PCC of the power plant for multi-generator SSR suppression purpose so that the investment costs are reduced while guaranteeing the requirements of the SSR damping.

More specifically, the control structure of SSRDS is proposed while its mathematical model is established. The damping torque analysis is presented theoretically to illustrate the impact factors of the SSR damping performance of SSRDS. Besides, to maximize the damping ability of SSRDS, parameters tuning method for mode filters and the gain and phase shift loops of the controller is well described in this paper. Finally, how the SSRDS behaves for a practical system, i.e., the Jinjie Power Plant, is fully analyzed in the case study. The effectiveness of the proposed controller under small disturbances and large disturbances is demonstrated through damping torque analysis, the eigenvalues analysis and the time-domain simulations.

II. SYSTEM CONFIGURATION AND ITS SSR CHARACTERISTIC

A. SYSTEM TOPOLOGY

To illustrate the effectiveness of the proposed control, the target system for investigation, i.e., the Jinjie series compensated transmission system is shown in Fig.1. The Jinjie Power Plant consists of four 600 MW rated SGs ($G_1 \sim G_4$) and two 660MW rated SGs ($G_5 \sim G_6$). The six generators are connected to the North China Grid via 500 kV transmission lines. In order to enhance the transferring capability, the fixed series capacitors are installed at the parallel transmission lines between Jinjie Power Plant, Xinzhou and Shibei with compensation degree of 35% and 40% as shown in Fig.1. The nearby Fugu power plant, which includes two 600 MW rated SGs and two 660MW rated SGs, is connected to the Xinzhou substation via two transmission lines with compensation degree of 35%. This paper focuses on the SSR problems of the six generators in the Jinjie Power Plant.

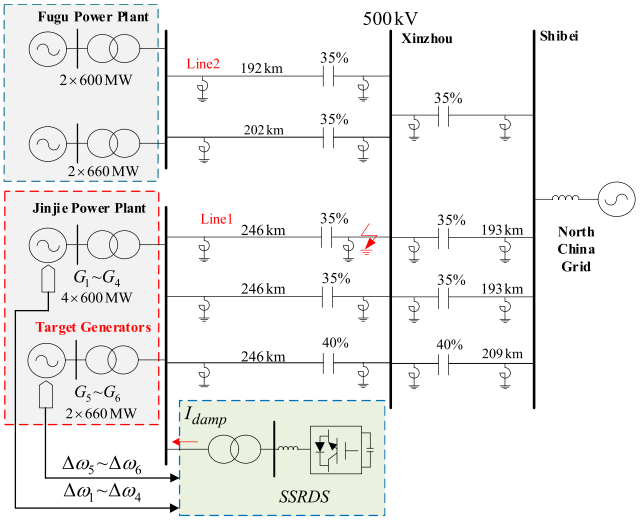

FIGURE 1. The single-line diagram of the Jinjie series compensated transmission system.

The multi-mass system of each SGs in Jinjie Power Plant consisting of the generator rotor, a high-intermediate-pressure (HIP) rotor and two low-pressure (LPA and LPB) rotors. To well describe the electromagnetic transient behaviors of SSR, the SGs are built by the detailed nine-order model in the following analysis. The excitation system is also implemented in SGs to improve the voltage stability of the power grid.

B. SSR ANALYSIS

For the targeted power grid shown in Fig.1, the system dynamics can be represented through series of differential equations by eliminating the algebraic vector [24], which can be expressed as,

$$\Delta \dot{\boldsymbol{x}} = A\Delta x \tag{1}$$

where, $\Delta \boldsymbol{x}$ is the vector of state variables, which consists of the states associated with the SGs and the power grid. $\boldsymbol{A}$ is the state matrix [29].

To perform eigenvalue analysis, the system (1) has been modeled in MATLAB software. Based on the eigenvalue calculation of the state matrices $\boldsymbol{A}$, the torsional modes (TMs) information of six generators in Jinjie Power Plant is listed in Table 1. It can be concluded from Table 1 that each generator has three natural sub-synchronous torsional modes. The TMs (TM1∼TM6) correlated to the shaft of the generators may potentially be excited during system disturbances, which finally leads to the unstable oscillation of the system when the damping ratios are not sufficient.

TABLE 1. The torsional modes of the generators.

Generator	Oscillation Frequency(Hz)		
	mode1	mode2	mode3
G_1~G_4	13.02 (TM1)	22.77 (TM2)	28.16 (TM3)
G_5~G_6	20.00 (TM4)	24.90 (TM5)	42.60 (TM6)

C. DAMPING TORQUE ANALYSIS

In order to adequately evaluate the damping characteristics of the target system and verify the eigenvalue analysis, the time-domain based electrical damping analysis [11] is carried out.

For a single generator, the small signal mathematical model of the electromagnetic torque is expressed as,

$$\Delta T_e = K_s \Delta\delta + D_e \Delta\omega \tag{2}$$

where, ΔT_e is the increment of the electromagnetic torque. K_s represents the synchronizing torque coefficient while D_e denotes the damping torque coefficient.

Transfer (2) into *Laplace* form and the transfer function of ΔT_e versus $\Delta\omega$ can be defined as follow [11], [24],

$$G_e(s) = \Delta T_e(s)/\Delta\omega(s) \tag{3}$$

Based on (3), the electrical damping factor can be easily obtained by,

$$D_e(\omega) = \mathrm{Re}\{G_e(j\omega)\} \tag{4}$$

The electrical damping torque analysis is performed in the PSCAD/EMTDC software under an operation condition that all the generator, transmission lines and series capacitors are in service. Its process is described as follows,

Step 1: A small perturbation signal at sub-synchronous range is added to the input mechanical torque of the generator, which will correspondingly excite the small deviation of rotor speed $\Delta\omega$ and electromagnetic torque ΔT_e. To decrease the impacts of the injected disturbances, the magnitude of the perturbation is approximately set as 0.01∼0.05p.u.

Step 2: The electrical damping factor D_e can be computed according to (4) in the concerned sub-synchronous range.

Step 3: If D_e is positive, the system is asymptotically stable. Otherwise, negative D_e will result in high risk of SSR.

It should be noticed that when calculating D_e of a specific generator, other non-concerned generators should be equivalent as the voltage source in order to get accurate results. As a result, the damping profiles of $G_1 \sim G_6$ are shown in Fig.2. It can be observed from Fig.5 that the electrical damping factors of TM1 (13.02Hz), TM3 (28.16Hz), TM5 (24.90Hz) and TM6 (42.60Hz) are negative. More specifically, TM3 of $G_1 \sim G_4$ and TM5 of $G_5 \sim G_6$ have the greater risk of SSR since their negative electrical damping peaks are higher than other TMs.

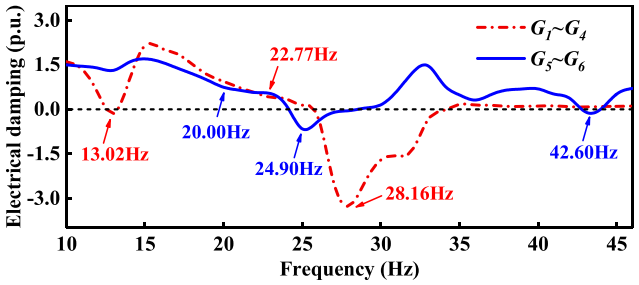

FIGURE 2. Electrical damping profile of G_1 to G_6.

III. PROPOSED VSC BASED SSR DAMPING CONTROL

Based on the above analysis, it's essential for making up novel control strategies to damp SSR in this multi-mode and multi-generator system. Therefore, a VSC based controller named SSRDS is proposed in this section. The control structure and the mathematical model of the proposed controller are fully illustrated. An analysis of auxiliary damping torque is presented, which can be used to quantify the contribution of SSRDS to the system damping.

A. CONTROL STRUCTURE OF SSRDS

The overall control structure of SSRDS is shown in Fig.3. The proposed controller consists of damping signal control loop, dq vector control loop and a voltage source converter.

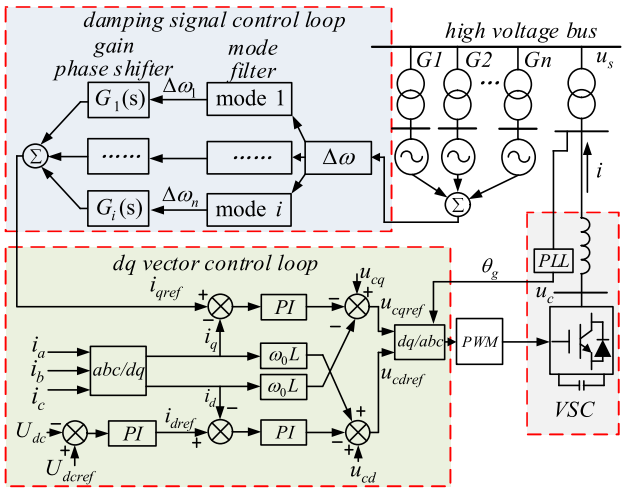

FIGURE 3. The overall control structure of SSRDS.

The rotor speed deviations of each generator which reflect the SSR modes are obtained by the measuring devices and are transmitted into the damping signal control loop of the nearby SSRDS located at the high voltage bus of the power plant. The impacts of the communication [30] are not discussed in this paper since the time delays of the communication infrastructure are small in this application scenario and they can be compensated by the phase shifter.

In the damping signal control loop, each TMs has its own processing path including the mode filter and the gain and phase shifter. The parameter design of the damping signal control loop will be presented in the next section. The typical dq vector control is adopted for VSC. The d-axis outer loop controls the DC-link voltage as constant, which are associated with d-axis current of the inner loop. The q-axis current reference of the inner loop i_{qref} is determined directly by the damping signal control loop, which is obtained by linearly superimposing all the TMs signals. The inner current loop will result in the good dynamic response of SSRDS. Furthermore, the pulse-width-modulation (PWM) technology is implemented in VSC for modulation.

In most of the existing references [25]–[28], the SSR dampers (SSDs) are placed at the generator terminal with low voltage rating, which means that one controller only takes effects on the one generator. This connecting method results in the direct control effect but may be expensive for the power plants with multi-generator for the following reasons. For practical applications, each controller should be equipped with several backup controllers for security purpose. Though the capacity of the SSDs in [25]–[28] are small, if considering all the backup controllers for the multi-generator power plants, the overall investment costs may be relatively high.

In the proposed control method, the SSRDS is placed at the PCC of the power plants with high voltage rating. As a result, the output damping current of SSRDS will be injected into each generator according to the *Kirchhoff Current Law* (*KCL*), which makes it possible to damp multi-generator and multi-mode SSR through single controller. More specifically, for the Jinjie Power Plants in the case study later on, one SSRDS rated at 40 MVA can stabilize SSR modes of six large-capacity generators by fully utilizing the capacity of the controller under elaborate design of the control parameters. Under this scheme, the number of backup controllers can also decrease and the overall investment costs will be less.

B. MODELING OF THE CONTROLLER

As shown in Fig.3., if the resistance is overlooked, the AC voltage equations of SSRDS at the three-phase frame is given by,

$$u_s - u_c = L\frac{di}{dt} \tag{5}$$

where, u_s and u_c are the AC voltage of the high voltage bus and converter voltage, respectively. L is the equivalent inductance. i represents the output current of SSRDS.

Convert (5) into d-axis and q-axis form,

$$\begin{cases} L\frac{di_d}{dt} = u_{sd} - u_{cd} + \omega_0 L i_q \\ L\frac{di_q}{dt} = u_{sq} - u_{cq} - \omega_0 L i_d \end{cases} \tag{6}$$

Considering the dynamic of the inner current controllers, (6) can be re-written as,

$$\begin{cases} u_{cd} = u_{sd} + K_{pd}(i_{dref} - i_d) + \int K_{id}(i_{dref} - i_d) - \omega_0 L i_q \\ u_{cq} = u_{sq} + K_{pq}(i_{qref} - i_q) + \int K_{iq}(i_{qref} - i_q) + \omega_0 L i_d \end{cases} \tag{7}$$

where, K_{pd}, K_{pq}, K_{id}, K_{iq} are the correlated parameters of the PI controller of the inner current control loop. The dynamics of the d-axis outer loop is not included in (7). It's reasonable since the response of the inner current loop is faster than that of the outer loop.

The exchanged active power P and the reactive power Q between the AC grid and the SSRDS can be expressed as,

$$P = u_{sd} i_d, \, Q = -u_{sd} i_q \tag{8}$$

As a result, P and Q are independently controlled by the dq vector control loop. When system is in the steady state, there is no power exchange between the SSRDS and the power grid. Once SSR occurs, the reactive damping current will be modulated for SSR damping support.

C. AUXILIARY DAMPING TORQUE ANALYSIS

The auxiliary damping torque provided by SSRDS is analyzed. Assume there is a small disturbance at frequency ω_i occurs on the rotor speed of the generator,

$$\Delta\omega = A_i \cos(\omega_i t) \tag{9}$$

where, A_i represents the magnitude of the perturbation. ω_i denotes the natural oscillation frequency of a certain TM.

Assume the phase shift of the mode filters can be well compensated, the q-axis current reference i_{qref} is,

$$i_{qref} = K_i A_i \cos(\omega_i t + \varphi_i) \tag{10}$$

where, K_i and φ_i are the correlated parameters of the gain and phase shifter.

The well-known park transformation can be expressed as,

$$i_{abc} = P^{-1} i_{dq0} \tag{11}$$

where, $i_{abc} = [i_a i_b i_c]^{\mathrm{T}}$ are the output current in abc-axis, $i_{dq0} = [i_d i_q \; i_0]^{\mathrm{T}}$ are the output current in dq-axis. $\boldsymbol{P}^{-1}$ is defined as follows,

$$\boldsymbol{P}^{-1} = \begin{bmatrix} \cos(\omega_0 t + \delta) & -\sin(\omega_0 t + \delta) & 1 \\ \cos(\omega_0 t + \delta - 2\pi/3) & -\sin(\omega_0 t + \delta - 2\pi/3) & 1 \\ \cos(\omega_0 t + \delta + 2\pi/3) & -\sin(\omega_0 t + \delta + 2\pi/3) & 1 \end{bmatrix} \tag{12}$$

where $(\omega_0 t + \delta)$ is the synchronous phase calculated by the phase locked loop (PLL) of SSRDS.

Due to the fast modulation capability of VSC, assume that i_d and i_q can ideally track the current reference, i.e., $i_d = i_{dref}$ and $i_q = i_{qref}$. According to (10), (11) and (12), the output *a-axis* current of SSRDS can be expressed as,

$$\begin{aligned} i_a &= K_i A_i \cos(\omega_i t + \varphi_i) \sin(\omega_0 t + \delta) \\ &= \frac{1}{2} K_i A_i \left[\sin((\omega_0 - \omega_i)t + \delta - \varphi_i) + \sin((\omega_0 + \omega_i)t + \delta + \varphi_i)\right] \\ &= i_{asub} + i_{a\,\mathrm{sup}} \end{aligned} \tag{13}$$

It can be observed from (13) that i_a is composed of sub-synchronous component i_{asub} at frequency $(\omega_0\text{-}\omega_i)$ and sup-synchronous component i_{asup} at frequency $(\omega_0 + \omega_i)$. As shown in Fig.3, the damping current generated by SSRDS will flow into the power grid based on *KCL*. From the perspective of the aimed generator, the injected current i_{Ga} can be derived as,

$$i_{Ga} = i_{Gasub} + i_{Gasup} \tag{14}$$

$$\begin{cases} i_{Gasub} = \dfrac{1}{2} k_{sub} K_i A_i \sin((\omega_0 - \omega_i)t + \delta - \varphi_i + \Delta\varphi_{sub}) \\ i_{Gasup} = \dfrac{1}{2} k_{sup} K_i A_i \sin((\omega_0 + \omega_i)t + \delta + \varphi_i + \Delta\varphi_{sup}) \end{cases} \tag{15}$$

where k_{sub}, k_{sup} are the current-division coefficient. $\Delta\varphi_{sub}$, $\Delta\varphi_{sup}$ are the phase shift considering the impacts of the transmission lines and the transformer.

For a certain generator, the relevant electromagnetic torque ΔT_e during system dynamic is given by [31],

$$\Delta T_e = \psi_{d0} \Delta i_q - \psi_{q0} \Delta i_d \tag{16}$$

where Ψ_{d0}, Ψ_{q0} are the initial value of flux linkage of the generator in dq frame, respectively. Δi_d, Δi_q are the current components in dq frame induced by the rotor oscillations.

Transform (III-C) into dq frame and combine with (16), the auxiliary electromagnetic damping torque ΔT_d provided by SSRDS is given as follows,

$$\Delta T_d = \Delta T_{dsub} + \Delta T_{dsup} \tag{17}$$

$$\begin{cases} \Delta T_{dsub} = \dfrac{1}{2} k_{sub} K_i A_i \psi_0 \sin(\omega_i t - \delta + \varphi_i - \Delta\varphi_{sub} - \theta_s) \\ \Delta T_{dsup} = -\dfrac{1}{2} k_{sup} K_i A_i \psi_0 \sin(\omega_i t + \delta + \varphi_i + \Delta\varphi_{sub} + \theta_s) \end{cases} \tag{18}$$

$$\psi_0 = \sqrt{\psi_{d0}^2 + \psi_{q0}^2}, \, \theta_s = \arctan(\psi_{d0}/\psi_{q0}) \tag{19}$$

According to (3) and (4), the electrical damping factor D_e contributed from SSRDS can be derived as,

$$\begin{aligned} D_e = &\frac{1}{2} k_{sub} K_i A_i \psi_0 \sin(-\delta + \varphi_i - \Delta\varphi_{sub} - \theta_s) \\ &- \frac{1}{2} k_{sup} K_i A_i \psi_0 \sin(\delta + \varphi_i + \Delta\varphi_{sup} + \theta_s) \end{aligned} \tag{20}$$

The maximum D_{emax} can be achieved if there is,

$$\begin{cases} \varphi_i = \dfrac{1}{2}(\Delta\varphi_{sub} + \Delta\varphi_{sup}) \\ \delta = -\dfrac{1}{2}(\pi + \Delta\varphi_{sub} + \Delta\varphi_{sup} + 2\theta_s) \end{cases} \tag{21}$$

$$D_{emax} = \frac{1}{2} K_i A_i \psi_0 (k_{sub} + k_{sup}) \tag{22}$$

It can be clearly observed from (20), (21) and (22) that the damping SSR performance of SSRDS is related to the current-division coefficient, steady state value of flux linkage of the generator, parameters of the gain and phase shifter and the phase shift caused by the power grid.

To well well explain the SSR damping mechanism of SSRDS, the vector diagram of ΔT_e is presented in Fig.4. The generator will have negative damping factor D_e if ΔT_e lags $\Delta\omega$ from $\pi/2$ to $3\pi/2$ as shown in red line, which may lead to the SSR problems. With the help of the auxiliary electromagnetic damping torque ΔT_d(marked as green in Fig.4.) provided by SSRDS, ΔT_e is adjusted to $\Delta T_e'$(marked as blue in Fig.4.), and the corresponding electrical damping factor D_e is greatly improved.

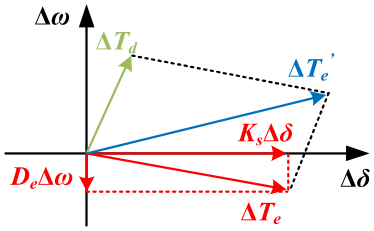

FIGURE 4. Vector diagram of ΔT_e.

IV. DESIGN OF THE PARAMETERS OF THE MODE FILTER AND THE GAIN AND PHASE SHIFT LOOP

Based on the above analysis, if the parameters of the damping signal control loop in Fig.5. are properly tuned, maximum damping support can be achieved by SSRDS. Therefore, the parameter tuning method of the mode filter, as well as the gain and phase shift are presented in this section to stimulate the potential of SSRDS.

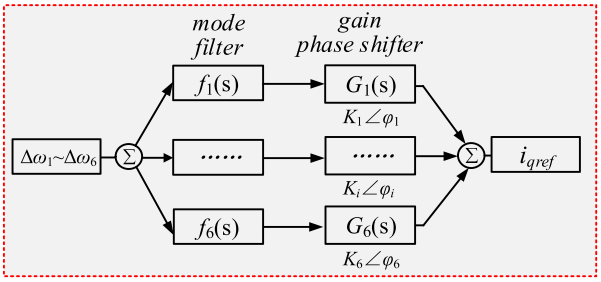

FIGURE 5. Diagram of the mode filter and the gain and phase shifter.

A. PARAMETER TUNE OF THE MODE FILTER

As shown in Fig.1, there are six generators and six TMs in the Jinjie Power Plant. For this test system, the well-designed mode filter should have the following characteristics: 1) The signal components which are correlated to the concerned TMs are supposed to be precisely extracted from the rotor speed deviations. 2) The mode filters should guarantee that the control signals of different TMs (especially for the TMs in close frequency range) should not interfere with each other and make sure the damping performance is not negatively affected by the interactions between different TMs. Therefore, for each TMs, eight cascading mode filters including a low-pass filter, a high-pass filter, a band-pass filter and five band-stop filter are adopted for signal processing. The transfer function $f_i(s)$ of the mode filter for a certain TM is described as,

$$f_i(s) = f_{L\&H}(s) \cdot f_{bp}(s) \cdot f_{bs}(s) \tag{23}$$

$$f_{L\&H}(s) = \frac{\omega_L^2}{s^2+\omega_L s+\omega_L^2}\frac{s^2}{s^2+\omega_H s+\omega_H^2} \tag{24}$$

$$f_{bp}(s) = \frac{\omega_i^2 s}{s^2+6\pi s+\omega_i^2} \tag{25}$$

$$f_{bs}(s) = \frac{\omega_{S1}^2+s^2}{s^2+6\pi s+\omega_{S1}^2}\frac{\omega_{S2}^2+s^2}{s^2+6\pi s+\omega_{S2}^2} + \frac{\omega_{S3}^2+s^2}{s^2+6\pi s+\omega_{S3}^2}\frac{\omega_{S4}^2+s^2}{s^2+6\pi s+\omega_{S4}^2}\frac{\omega_{S5}^2+s^2}{s^2+6\pi s+\omega_{S5}^2} \tag{26}$$

where $f_{L\&H}(s)$, $f_{bp}(s)$ and $f_{bs}(s)$ are the transfer functions of low-pass and high-pass filter, band-pass filter and band-stop filter. ω_L is set as $2\pi*47$, while ω_L is $2\pi*10$, which enabling only the interested sub-synchronous components (10∼47Hz) to pass through. ω_i is the frequency of the concerned TM. ω_{S1} to ω_{S5} represent the frequency of other five TMs to be inhibited. The corresponding bode diagram of the six mode filters are shown in Fig.6 and Fig.7. The correlated frequency of each TMs as concluded in Table 1 are marked as f_{TM1} to f_{TM6}, respectively.

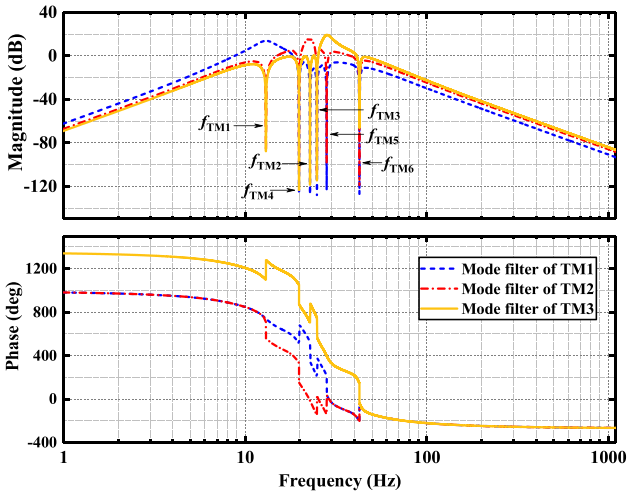

FIGURE 6. Frequency response of the mode filters of TM1 to TM3.

B. PARAMETER TUNE OF THE GAIN AND PHASE SHIFTER

As it is analyzed in section III, the parameters of the gain and phase shifter are of high importance in achieving the best

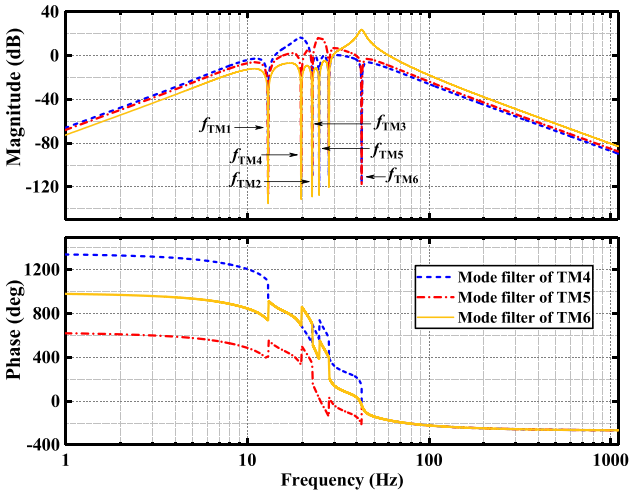

FIGURE 7. Frequency response of the mode filters of TM4 to TM6.

damping performance of SSRDS. For each torsional mode, the transfer function $G_i(\mathrm{s})$ of the its gain and phase shifter is,

$$G_i(\mathrm{s}) = K_i \cdot \left(\frac{1+T_i s}{1-T_i s}\right)^2 = K_i \angle \varphi_i \tag{27}$$

$$\varphi_i = 4 \cdot \arctan(T_i \cdot \omega_i) \tag{28}$$

where, T_i ($i = 1, \ldots, 6$) are the time constant, K_i and φ_i ($i = 1, \ldots, 6$) are the gain coefficient and the phase shifter angle of each TMs.

The parameters of the gain and the phase shifter parameters should guarantee that all the SSR modes are well stabilized under various operating conditions, especially for the SSR modes with poor damping property. Theoretically, the optimal phase shifter angles φ_i can be computed by (21) and the gain factors K_i can be set as large as possible to reach maximum positive damping factor as indicated in (22). However, it is relatively time-consuming to resolve the equation (21) for practical applications since the power grid described in Fig.1 is a nonlinear system. At the same time, considering the rated capacity constraint of SSRDS and the impacts of the limiter of the control loop, the gain factors K_i are supposed to be set within a reasonable range. Based on the above concerns, the detailed control-design process of the gain and the phase shift parameters is given as follows:

Step 1: The typical operating conditions selection. The frequency scanning method is utilized to roughly select the operation conditions with poor damping performance. Due to its fast calculation ability, 80 representative operating conditions is quickly selected as the ''evaluation conditions'' by making compromises among different conditions.

Step 2: Modeling of the nonlinear optimization problem. To stabilize all the SSR modes in Jinjie Power Plants, there are 6 sets of K_i and φ_i (i = 1, . . . ,6) to be optimized. According to [4], the fitness function and the mathematical model of this optimization problem can be defined as,

$$\begin{cases} f = \sum_{i=1}^{6} w_i \eta_i + w_7 \min\{\eta_1, \eta_2, \eta_3\} + w_8 \min\{\eta_4, \eta_5, \eta_6\} \\ \eta_i = \min_{j=1} \{\sigma_{ij}\}, \sigma_{ij} = -\mathrm{Re}(\lambda_{ij}) / \left|\mathrm{Im}(\lambda_{ij})\right| \\ \lambda_{ij} = \boldsymbol{Eig}\left\{\boldsymbol{A}_j(K_1, \ldots, K_i, \theta_1, \ldots, \theta_i)\right\}, \\ \qquad i = 1, \ldots, 6; j = 1, \ldots, 80 \end{cases} \tag{29}$$

$$\begin{cases} \max f \\ \text{subject to} : |K_i| \le K_i^{\max}, |\varphi_1| \le \varphi_i^{\max} \end{cases} \tag{30}$$

where the subscripts i and j denote the number of SSR modes and the evaluation conditions, respectively. $\boldsymbol{A}_j$ represent the state matrices defined by (1). $\boldsymbol{Eig}\{\}$ is the computation of the eigenvalues of each $\boldsymbol{A}_j$ while the λ_{ij} is the eigenvalues under a certain operating condition. $\mathrm{Re}(\lambda_{ij})$ and $\mathrm{Im}(\lambda_{ij})$ are the real and imaginary parts of the λ_{ij}. σ_{ij} are the damping ratios. η_i is the minimum damping ratios values among the evaluation conditions. w_i is the weight coefficient. Based on the electrical damping torque analysis in Section II, C, the weight coefficient can be set as: $w_1 = w_2 = w_3 = w_4 = w_5 = w_6 = 0.08$, $w_7 = 0.32$, $w_8 = 0.16$. K_i^{max} and φ_i^{max} are the upper bounds of the gains and phase shifter, respectively.

Step 3: Solve (29) and (30) by using the genetic algorithm and simulated annealing (GA-SA) algorithm. The optimization problem described in (29) and (30) is a nonlinear optimization problem with multi-dimension, which it's relatively difficult to handle for the traditional linear optimization method. Therefore, the modern optimization method proposed in [4], i.e., the GA-SA algorithm is adopted to search the optimal control parameters. This combined algorithm effectively eliminates the limitations of the inherent shortcomings of two individual algorithms. As a result, the GA-SA is less sensitive to the parameters and has better convergence performance, which largely improves the computational efficiency. In this case, the GASA converges to satisfactory results after 40-60 iterations.

Step 4: Time-domain simulations verification. The optimization results can be tested in the PSCAD to verify the effectiveness of the above parameters tuning method. If the optimization results are not perfect enough, the parameters in the optimization model can be modified and *step* 1 to *step* 4 can be performed again until the satisfactory results appear.

The final gain and phase shifter parameters adopted in the case study later on are listed: $K_1 = 12.35$, $\varphi_1 = 1.484$rad, $K_2 = 4.66$, $\varphi_2 = 1.309$rad, $K_3 = 50.41$, $\varphi_3 = 1.396$rad, $K_4 = 4.37$, $\varphi_4 = 1.134$rad, $K_5 = 21.79$, $\varphi_5 = 1.221$rad, $K_6 = 14.68$, $\varphi_6 = 1.293$rad. Certainly, there are other alternative approaches to tune the parameters, but it is outside scope of this paper. Under the designed mode filter and the gain and the phase shifter, the SSRDS will be activated only when the SSR appears in the system. During normal operation, the proposed damper will have little impacts on the stability of the power grid.

V. CASE STUDIES

To demonstrate the effective SSR damping ability of SSRDS, the nonlinear time-domain simulations considering small disturbances and large disturbances are performed in PSCAD/EMTDC software. The detailed electromagnetic transient simulation model as shown in Fig.1 are established. The damping performance of SSRDS is also compared with traditional SVC-SSDC.

As an important parameter, the SSRDS power rating has significant effect on the tuning of the gain coefficients and the damping performance of the controller. For practical application, the rated capacity of SSRDS should be tuned based on the following principles: 1) the SSRDS with minimum power rating should at least simultaneously stabilize all the SSR modes of the target system; 2) the SSRDS under designed power rating and the gain coefficients should guarantee that the control output is not clipped under both normal operation and SSR events; 3) the operating margin and the equipment costs need to be balanced. According to the previously mentioned principles, the rated capacity of SSRDS is set as 40MVA for the Jinjie Power Plant, which is achievable and cost-less for the practical application. To simultaneously stabilize all the SSR modes, the SSRDS rated at 40MVA is placed at the common bus of Jinjie Power Plant with 500kV voltage rating as indicted in Fig.1. The other correlated parameters of SSRDS are listed in Table 2.

TABLE 2. The parameters of SSRDS.

Item	Value
Rated capacity	40 MVA
Reactor	5.848 mH
DC-link capacitor of each H-bridge	8400 μF
DC voltage	2200 V
Number of H-bridge	15 per phase
Frequency of PWM	350 Hz
	35 kV/550 kV
Dedicated transformer	Δ/Y
	X_{leak}=12%

A. DAMPING PERFORMANCE UNDER SMALL DISTURBANCES

If the system disturbances are relatively tiny, the linearized models of the system are theoretically effective. Therefore, the SSR damping capability of the SSRDS under small disturbances is analyzed here by using eigenvalue analysis and damping torque analysis. A typical operation condition is implemented in the following analysis, where all the units and the transmission lines of the Jinjie Power Plant are in service as shown in Fig.1.

The small signal model of the system described in (1) is well established in MATLAB software and the relevant eigenvalues of the system with and without SSRDS are summarized in Table 3. It can be clearly observed from Table 3 that the real parts of TM3 and TM5 are positive when the SSRDS is out of service, which might cause high risks of unstable

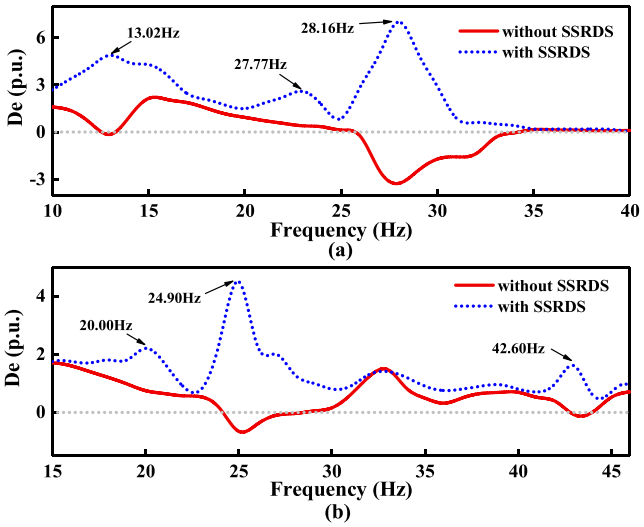

FIGURE 8. Electrical damping profile of (a) G_1~G_4; (b) G_5~G_6.

TABLE 3. Relevant eigenvalues of the system.

TM	Without SSRDS $\sigma \pm j\omega$	With SSRDS $\sigma \pm j\omega$
TM1	-0.035±*j*81.807	-0.163±*j*81.823
TM2	-0.146±*j*143.068	-0.151±*j*143.072
TM3	+0.320±*j*176.934	-0.427±*j*176.986
TM4	-0.131±*j*125.664	-0.186±*j*125.676
TM5	+0.089±*j*156.451	-0.513±*j*156.462
TM6	-0.002±*j*267.664	-0.127±*j*267.679

SSR. However, TM3 and TM5 exhibit the negative real parts if the SSRDS is in operation, which verifies that the proposed SSRDS can effectively damp SSR of multi-generator and multi-mode.

To get further insight into the damping support provided by SSRDS and demonstrate the correctness of the eigenvalues analysis, the time-domain based auxiliary damping torque analysis is performed in PSCAD/EMTDC. By injecting a series of perturbation with sub-synchronous frequency range into the mechanical torque of the concerned generator, the auxiliary damping torque can be computed based on (4) and (5). Correspondingly, the electrical damping profiles for the target generators with SSRDS are shown in Fig.8. As it is observed, when the SSRDS is applied, the electrical damping of the generators is significantly improved in sub-synchronous frequency range, especially for the TMs with negative damping ratio.

The results again demonstrate the effectiveness of the proposed controller.

B. SIMULATION RESULTS UNDER LARGE DISTURBANCES

In daily operation, the power grid will inevitably suffer from large disturbances. Therefore, it's indispensable to test whether the SSRDS is robust enough under large disturbances. For practical power systems, there exist many factors that can trigger SSR. In this paper, the most serious disturbance, i.e., the short-circuit fault event is adopted to trigger SSR. To further evaluate the performance of the proposed

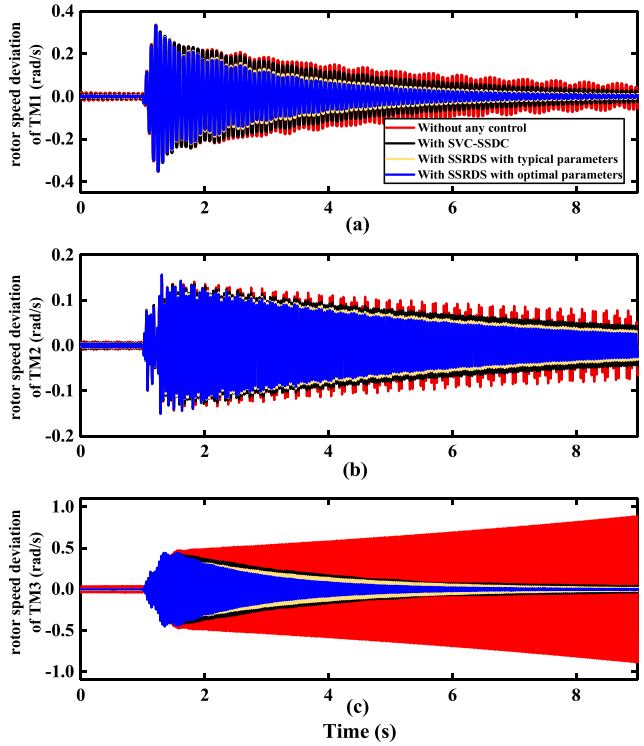

FIGURE 9. Dynamic responses of the rotor speed deviation of TM1 to TM3 under Case 2.

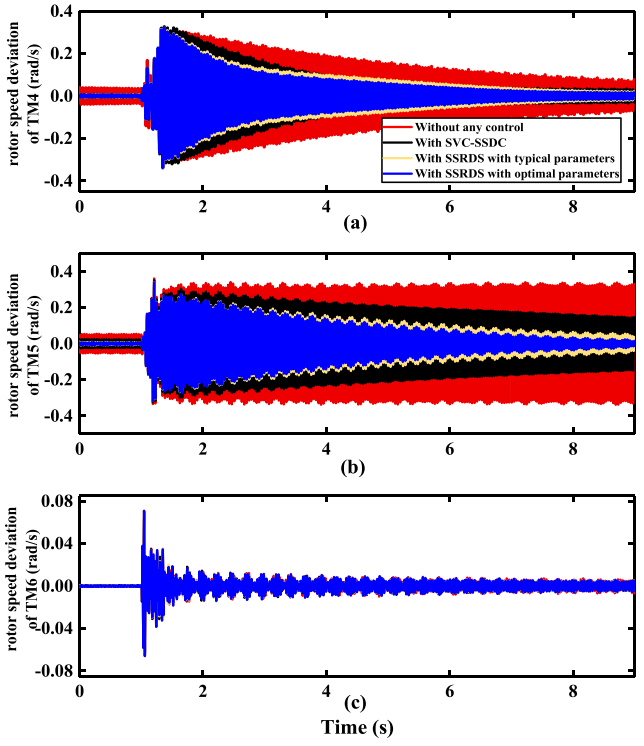

FIGURE 10. Dynamic responses of the rotor speed deviation of TM4 to TM6 under Case 1.

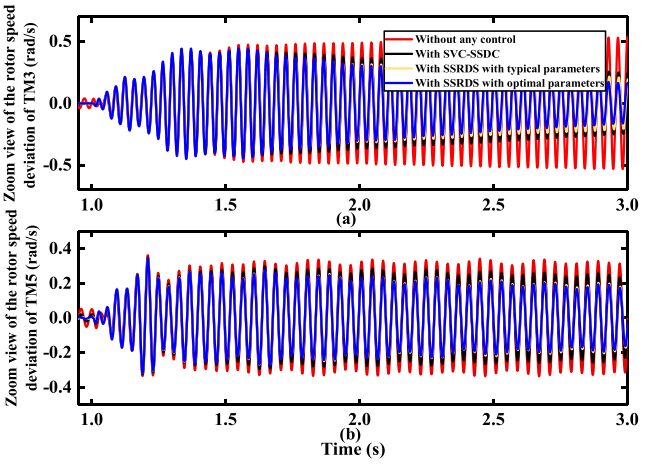

FIGURE 11. The zoom view of the dynamic responses of the rotor speed deviation of TM3 and TM5 under Case 1.

SSRDS under various operating conditions, the frequency scanning method is utilized to select the evaluation conditions. Two typical serious operating conditions are performed in PSCAD:

Case 1: All the units including the generators, the series capacitors and the transmission lines of the Jinjie Power Plant are in service as shown in Fig.1. The output level of each generator reaches to 0.5 p.u. The single-phase-to-ground fault is adopted.

Case 2: The transmission Line 2 in the Fig.1 is disconnected, other units are all in service. The output level of each generator reaches to 0.5 p.u. The most critical fault, i.e, the three-phase fault is employed.

Four different scenarios, namely, without any control, with SVC-SSDC, with SSRDS with typical parameters and with SSRDS with optimal parameters are compared in detail in the simulation studies. The SVC-SSDC proposed in [4], [24] is an early SSR mitigation solution for the Jinjie Power Plant. To fully evaluate the damping performance of the proposed control scheme in the Jinjie Power Plant, the simulation results of SSRDS are compared with the previously adopted SVC-SSDC. The SVC-SSDC model employed in the simulations is referring to [4]. And its rated capacity is set as 120MVA. The impacts of the parameters of the gain and phase shifter of SSRDS are investigated. The optimal parameters are tuned according to the optimization processes described in section IV, while the typical parameters are set based on the experiences without optimization procedures.

1) CASE 1

Fig.9, Fig.10 and Fig.11 show the dynamic responses of the rotor speeds of the six generators under single-phase-to-ground fault at Line 1 near the Xinzhou bus as shown in Fig.1. The fault is triggered at $t = 1$s and has a duration of 0.1s. Fig.11 is the zoom view of the dynamic responses of the rotor speed deviation of two SSR modes with negative damping, i.e., TM3 and TM5.

As it is clearly evidenced in Fig.9, Fig.10 and Fig.11, the system dynamic performances following short-circuit fault clearance is compromised by SSR. The rotor speed deviations of TM1, TM2, TM4 and TM6 can maintain stable

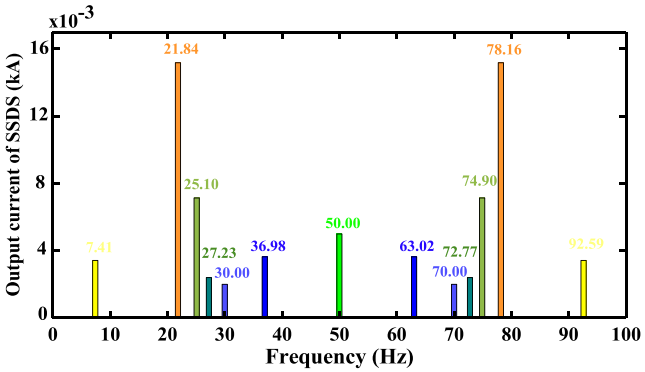

FIGURE 12. FFT analysis of the output current of SSRDS.

after large disturbance while they exhibit continuously unstable oscillations for TM3 and TM5 if there are no control schemes. The results are consistent with the eigenvalue analysis summarized in Table 3 and the damping profile analysis shown in Fig.8, respectively. However, both SVC-SSDC and SSRDS can take effects on the mitigation of the SSR for this six-generator and six-mode system. The oscillation amplitudes of TM1∼TM6 all decrease during system dynamics when the SVC-SSDC or SSRDS are in operation, especially for TM3 and TM5, which have negative damping.

Furthermore, it can be observed from Fig.9, Fig.10 and Fig.11 that, the control scheme of SSRDS with optimal parameters can achieve best damping performance, followed by SSRDS with typical parameter and SVC-SSDC. The results indicate that SSRDS can get better SSR damping characteristics at the expense of less capacity compared with SVC-SSDC. This is not unreasonable for the following reasons: 1) due to the half-controlled thyristors of the SVC-SSDC, the modulation capability of SVC-SSDC is worse than VSC. It will take extra prices for SVC-SSDC to modulate six sets of sub-synchronous and sup-synchronous damping currents, which results in the slower response speed compared to full-controlled VSC based SSRDS; 2) during system dynamics, the unexpected harmonic current [4] will be inevitably produced by SVC-SSDC, which might lead to the waste of the effective capacity. Fig.12 shows the result of the fast Fourier transform (FFT) of the output current of SSRDS during system disturbances. As it is illustrated, six groups of symmetric sub and super-synchronous currents related to the six TMs are modulated by SSRDS and will be injected into generator to produce positive electrical damping torque, which verifies analytical result in equation (13). Only a small amount of fundamental current is generated by SSRDS for stabilizing DC-link voltage of the VSC, so the capacity of SSRDS is well utilized.

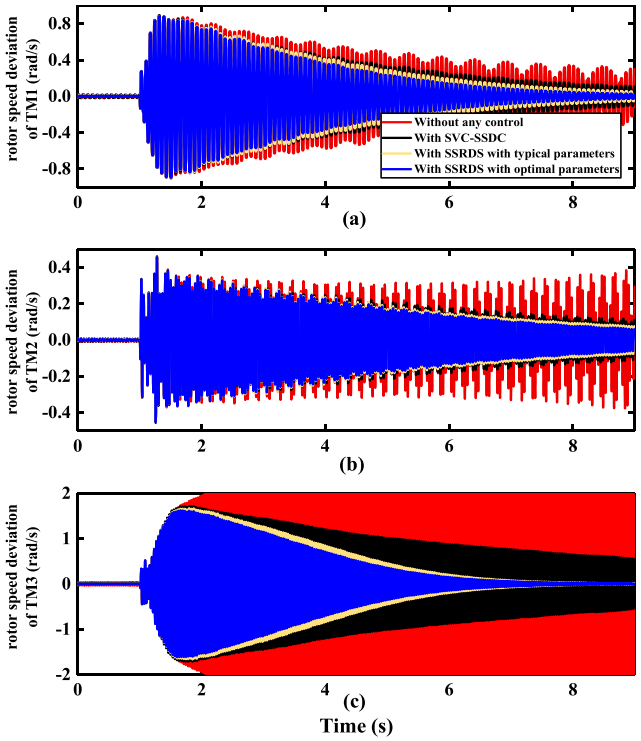

FIGURE 13. Dynamic responses of the rotor speed deviation of TM1 to TM3 under Case 2.

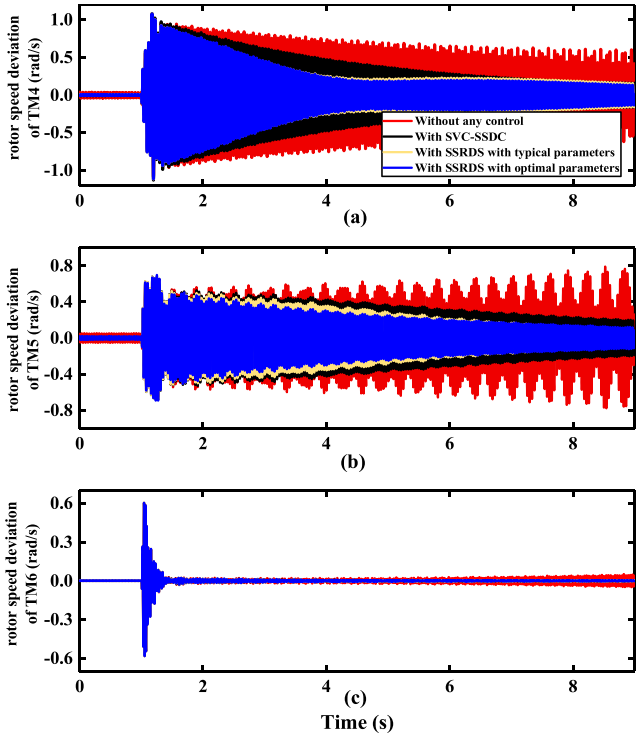

FIGURE 14. Dynamic responses of the rotor speed deviation of TM4 to TM6 under Case 2.

2) CASE 2

Fig.13, Fig.14 and Fig.15 show the simulation results under a critical operating condition (Case 2), where the most serious fault, i.e, the three-phase fault, is triggered at Line 1 near Xinzhou bus as shown in Fig.1. The fault happened at $t = 1$s and the transmission Line 1 was cut off after 0.1s.

It can be observed from Fig.13, Fig.14 and the zoom view in Fig.15 that the peak values of the rotor speed deviations of

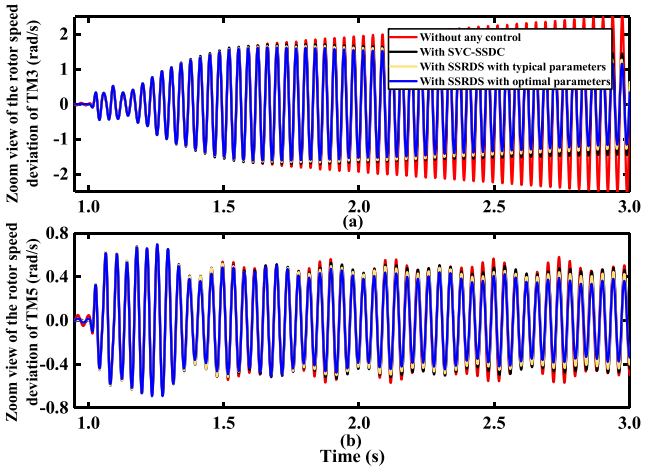

FIGURE 15. The zoom view of the dynamic responses of the rotor speed deviation of TM3 and TM5 under Case 2.

all the TMs are higher than that in Case 1 during the fault. This can be well explained that the energy shock during system dynamic from the three-phase fault is much larger than the single-phase fault. This transient energy shock might cause the shaft fatigue or even the shaft fatigue failure in some critical operating conditions, which may active the protective infrastructures and trip the generator in practical power systems. Correspondingly, the excited torsional oscillations are much more intense, especially for TM3 and TM5. It's worth noticing that TM2 cannot maintain stable and will experience an obvious oscillation after the disturbances without any control, which is different from Case 1. This verify the facts that the damping ratio of each TMs varies from one operating condition to another.

However, the damping profile of all TMs are improved and the SSR modes are well stabilized under both SVC-SSDC and SSRDS as obviously illustrated in the simulation results. The SSRDS with optimal parameters still realizes the best damping performance among all the control schemes, which verify the rationality and the robustness of the proposed parameters tuning method under different operating conditions.

To sum up, the analytical and simulation results under Case 1 and Case 2 of this section have fully demonstrated the effectiveness and the superiority of the proposed SSRDS for multi-generator and multi-mode SSR suppression under both small and large disturbances.

VI. CONCLUSION

This paper proposes an effective VSC based controller, named SSRDS, for multimodal SSR suppression. The SSRDS is composed of a damping signal control loop, a *dq* vector control loop and a voltage source converter. The SSR suppression mechanism of SSRDS is illustrated through damping torque analysis. Besides, the control parameters tuning method is presented to avoid the negative affects between the different TMs as well as optimize the damping effects of SSRDS. The SSRDS can exert positive damping support on the generators to suppress SSR, which is proved by time-domain based damping torque analysis and eigenvalues analysis. The simulation results have showed that the output damping currents of SSRDS consist of six groups of symmetric sub and super-synchronous components during system dynamics. As a result, the six-mode SSR of six generators in Jinjie Power Plant is well mitigated by one proposed controller. Compared to SVC-SSDC, the SSRDS can achieve better SSR damping performance at the expense of less rated capacity. The proposed SSRDS can also be applied into other application scenarios with the similar topology to Jinjie Power Plant.

REFERENCES

[1] *NETS SQSS and Grid Code GSR018/GC0077: Sub-Synchronous Oscillations (SSO)*, National Grid, Warwick, London, U.K., Mar. 2017.
[2] L. Livermore, Q. Mu, J. B. Ekanayake, C. E. Ugalde-Loo, J. Liang, and N. Jenkins, "Damping of subsynchronous resonance using a voltage source converter-based high-voltage direct-current link in a series-compensated great britain transmission network," *IET Gener., Transmiss. Distrib.*, pp. 542–551, Jan. 2014.
[3] IEEE Subsynchronous Resonance Working Group, "Terms, definitions and symbols for subsynchronous oscillations," *IEEE Trans. Power App. Syst.*, vol. PAS-104, no. 6, pp. 1326–1334, Jun. 1985.
[4] X. Xie, Q. Jiang, and Y. Han, "Damping multimodal subsynchronous resonance using a static var compensator controller optimized by genetic algorithm and simulated annealing," *Eur. Trans. Electr. Power*, vol. 22, no. 8, pp. 1191–1204, Nov. 2012.
[5] J. F. Hauer, W. A. Mittelstadt, R. J. Piwko, B. L. Damsky, and J. D. Eden, "Modulation and SSR tests performed on the BPA 500 kV thyristor controlled series capacitor unit at slatt substation," *IEEE Trans. Power Syst.*, vol. 11, no. 2, pp. 801–806, May 1996.
[6] L. Wang, H.-R. Liang, A. V. Prokhorov, H. Mokhlis, and C. K. Huat, "Modal control design of damping controllers for thyristor-controlled series capacitor to stabilize common-mode torsional oscillations of a series-capacitor compensated power system," *IEEE Trans. Ind. Appl.*, vol. 55, no. 3, pp. 2327–2336, May 2019.
[7] D.-J. Kim, H.-K. Nam, and Y.-H. Moon, "A practical approach to HVDC system control for damping subsynchronous oscillation using the novel eigenvalue analysis program," *IEEE Trans. Power Syst.*, vol. 22, no. 4, pp. 1926–1934, Nov. 2007.
[8] Y. Li, J. Li, L. Xiong, X. Zhang, and Z. Xu, "DC fault detection in meshed MTdc systems based on transient average value of current," *IEEE Trans. Ind. Electron.*, vol. 67, no. 3, pp. 1932–1943, Mar. 2020.
[9] T. Joseph, C. E. Ugalde-Loo, S. Balasubramaniam, and J. Liang, "Real-time estimation and damping of SSR in a VSC-HVDC connected series-compensated system," *IEEE Trans. Power Syst.*, vol. 33, no. 6, pp. 7052–7063, Nov. 2018.
[10] T. Joseph, C. E. Ugalde-Loo, S. Balasubramaniam, J. Liang, and G. Li, "Experimental validation of an active wideband SSR damping scheme for series-compensated networks," *IEEE Trans. Power Del.*, vol. 35, no. 1, pp. 58–70, Feb. 2020.
[11] K. M. Alawasa and Y. A.-R.-I. Mohamed, "A simple approach to damp SSR in series-compensated systems via reshaping the output admittance of a nearby VSC-based system," *IEEE Trans. Ind. Electron.*, vol. 62, no. 5, pp. 2673–2682, May 2015.
[12] P. Mahish and A. K. Pradhan, "Mitigating subsynchronous resonance using synchrophasor data based control of wind farms," *IEEE Trans. Power Del.*, vol. 35, no. 1, pp. 364–376, Feb. 2020.
[13] C. Karunanayake, J. Ravishankar, and Z. Y. Dong, "Nonlinear SSR damping controller for DFIG based wind generators interfaced to series compensated transmission systems," *IEEE Trans. Power Syst.*, vol. 35, no. 2, pp. 1156–1165, Mar. 2020.
[14] P. Li, L. Xiong, F. Wu, M. Ma, and J. Wang, "Sliding mode controller based on feedback linearization for damping of sub-synchronous control interaction in DFIG-based wind power plants," *Int. J. Electr. Power Energy Syst.*, vol. 107, pp. 239–250, May 2019.
[15] X. Zhang, X. Xie, H. Liu, and Y. Li, "Robust subsynchronous damping control to stabilise SSR in series-compensated wind power systems," *IET Gener., Transmiss. Distrib.*, vol. 13, no. 3, pp. 337–344, Feb. 2019.

[16] C. E. J. Bowler, D. H. Baker, N. A. Mincer, and P. R. Vandiveer, "Operation and test of the navajo SSR protective equipment," *IEEE Trans. Power App. Syst.*, vol. PAS-97, no. 4, pp. 1030–1035, Jul. 1978.
[17] X. Xie, P. Liu, K. Bai, and Y. Han, "Applying improved blocking filters to the SSR problem of the tuoketuo power system," *IEEE Trans. Power Syst.*, vol. 28, no. 1, pp. 227–235, Feb. 2013.
[18] S. Wang, Z. Xu, and F. Xing, "Application of bypass damping filter in suppressing subsynchronous resonance of multi-generator series-compensated systems," *Electr. Power Syst. Res.*, vol. 168, pp. 117–126, Mar. 2019.
[19] X. Xie, H. Liu, and Y. Han, "SEDC's ability to stabilize SSR: A case study on a practical series-compensated power system," *IEEE Trans. Power Syst.*, vol. 29, no. 6, pp. 3092–3101, Nov. 2014.
[20] X. Xie, L. Wang, and Y. Han, "Combined application of SEDC and GTSDC for SSR mitigation and its field tests," *IEEE Trans. Power Syst.*, vol. 31, no. 1, pp. 769–776, Jan. 2016.
[21] P. Dattaray, D. Chakravorty, P. Wall, J. Yu, and V. Terzija, "A novel control strategy for subsynchronous resonance mitigation using 11 kV VFD-based auxiliary power plant loads," *IEEE Trans. Power Del.*, vol. 33, no. 2, pp. 728–740, Apr. 2018.
[22] K. R. Padiyar and N. Prabhu, "Design and performance evaluation of subsynchronous damping controller with STATCOM," *IEEE Trans. Power Del.*, vol. 21, no. 3, pp. 1398–1405, Jul. 2006.
[23] M. S. El-Moursi, B. Bak-Jensen, and M. H. Abdel-Rahman, "Novel STATCOM controller for mitigating SSR and damping power system oscillations in a series compensated wind park," *IEEE Trans. Power Electron.*, vol. 25, no. 2, pp. 429–441, Feb. 2010.
[24] X. Zhu, H. Sun, J. Wen, and S. Cheng, "Improved complex torque coefficient method using CPCM for multi-machine system SSR analysis," *IEEE Trans. Power Syst.*, vol. 29, no. 5, pp. 2060–2068, Sep. 2014.
[25] L. Wang, X. Xie, Q. Jiang, and H. R. Pota, "Mitigation of multimodal subsynchronous resonance via controlled injection of supersynchronous and subsynchronous currents," *IEEE Trans. Power Syst.*, vol. 29, no. 3, pp. 1335–1344, May 2014.
[26] X. Xie, L. Wang, X. Guo, Q. Jiang, Q. Liu, and Y. Zhao, "Development and field experiments of a generator terminal subsynchronous damper," *IEEE Trans. Power Electron.*, vol. 29, no. 4, pp. 1693–1701, Apr. 2014.
[27] J. Zhang, X. Xiao, P. Zhang, C. Luo, Y. Wu, J. Lu, and L. Ren, "Suppressing intermittent subsynchronous oscillation via subsynchronous modulation of reactive current," *IEEE Trans. Power Del.*, vol. 30, no. 5, pp. 2321–2330, Oct. 2015.
[28] X. Xiao, Y. Wu, W. Yang, J. Zhang, and C. Luo, "Analysis of frequently over-threshold subsynchronous oscillation and its suppression by subsynchronous oscillation dynamic suppressor," *IET Gener., Transmiss. Distrib.*, vol. 10, no. 9, pp. 2127–2137, Jun. 2016.
[29] G. Wu, Z. Du, C. Li, and G. Li, "VSC-MTDC operation adjustments for damping inter-area oscillations," *IEEE Trans. Power Syst.*, vol. 34, no. 2, pp. 1373–1382, Mar. 2019.
[30] C. Li, J. Wu, C. Duan, and Z. Du, "Development of an effective model for computing rightmost eigenvalues of power systems with inclusion of time delays," *IEEE Trans. Power Syst.*, vol. 34, no. 6, pp. 4216–4227, Nov. 2019.
[31] I. M. Canay, "A novel approach to the torsional interaction and electrical damping of the synchronous machine part II: Application to an arbitrary network," *IEEE Trans. Power App. Syst.*, vol. PAS-101, no. 10, pp. 3639–3647, Oct. 1982.

XIAOTIAN YUAN (Student Member, IEEE) received the B.S. degree in electrical engineering from Xi'an Jiaotong University, Xi'an, China, in 2017, where he is currently pursuing the Ph.D. degree. His research interests include power system stability and control.

ZHENGCHUN DU (Senior Member, IEEE) was born in Shaanxi, China, in 1963. He received the B.S., M.S., and Ph.D. degrees in electrical engineering from Xi'an Jiaotong University, Xi'an, China, in 1983, 1986, and 1993, respectively. He is currently a Professor of electrical engineering with Xi'an Jiaotong University. His research interests include power system stability and control.

XIAOFANG WU received the B.S. degree in electrical engineering from Chongqing University, Chongqing, China, in 2017. She is currently pursuing the Ph.D. degree with Xi'an Jiaotong University. Her research interests include power system stability and stability analysis of renewable energy grid connection systems.

GUIHONG WU is currently pursuing the Ph.D. degree with Xi'an Jiaotong University. His research interests include power system stability and control of HVDC transmission.

SHUAI GAO received the B.S. degree in electrical engineering from Xi'an Jiaotong University, Xi'an, China, in 2016, where he is currently pursuing the Ph.D. degree. His research interests include power system stability and control.

FENG ZENG received the B.S. degree in electrical engineering from Xi'an Jiaotong University, Xi'an, China, in 2018, where he is currently pursuing the M.S. degree. His research interests include stability analysis and control of wind power systems.

CHONGTAO LI received the Ph.D. degree in electrical engineering from Xi'an Jiaotong University, Xi'an, China, in 2013. He is currently an Associate Professor of electrical engineering with Xi'an Jiaotong University. His research interests include power system stability and control.